ANL-6985

Argonne National Laboratory

A CONVECTIVE-DIFFUSION STUDY OF THE DISSOLUTION KINETICS OF 304 STAINLESS STEEL IN THE BISMUTH-TIN EUTECTIC ALLOY

by

T. F. Kassner

Al-

your request

of 10/22/74.

When no longer

needed return to

Library - No more

Copies available.

Ed Lebray

Printed in USA. Price $2.00. Available from the Clearinghouse for Federal Scientific and Technical Information, National Bureau of Standards, U. S. Department of Commerce, Springfield, Virginia

ANL-6985
Chemistry (TID-4500)
AEC Research and
Development Report

ARGONNE NATIONAL LABORATORY
9700 South Cass Avenue
Argonne, Illinois 60439

A CONVECTIVE-DIFFUSION STUDY OF THE DISSOLUTION KINETICS OF 304 STAINLESS STEEL IN THE BISMUTH-TIN EUTECTIC ALLOY

by

T. F. Kassner

Metallurgy Division

Metallurgy Program 8.2.4

Portions of this material have appeared in
ANL-7000, pp. 133-134 (1964)

November 1965

Operated by The University of Chicago
under
Contract W-31-109-eng-38
with the
U. S. Atomic Energy Commission

TABLE OF CONTENTS

	Page
ABSTRACT	7
INTRODUCTION	7
KINETICS OF DISSOLUTION	8
CONVECTIVE DIFFUSION IN LIQUIDS	9
EXPERIMENTAL METHOD	19
RESULTS	20
DISCUSSION	24
SUMMARY AND CONCLUSIONS	28
APPENDIXES	
A. Chemical Analysis for the 304 SS Sample Material	29
B. Chemical-analysis Data for the Dissolution Runs	30
C. Equilibrium-solubility Data for 304 SS in the Bi-42w/oSn Eutectic Alloy	39
ACKNOWLEDGMENT	40
REFERENCES	41

LIST OF FIGURES

No.	Title	Page
1.	Schematic Representation of Flow Lines near the Surface of a Rotating Disc	10
2.	Graph of the Functions $F(\xi)$, $G(\xi)$, and $-H(\xi)$	11
3.	Schematic Diagram of the Dissolution Apparatus	19
4.	Temperature Dependence of the Solubility of Iron from 304 SS in the Bismuth-Tin Eutectic Alloy	21
5.	Temperature Dependence of the Solubility of Chromium from 304 SS in the Bismuth-Tin Eutectic Alloy	21
6.	Temperature Dependence of the Solubility of Nickel from 304 SS in the Bismuth-Tin Eutectic Alloy	21
7.	Temperature Dependence of the Solubility of Manganese from 304 SS in the Bismuth-Tin Eutectic Alloy	21
8.	Temperature Dependence of the Solubility of 304 SS in the Bismuth-Tin Eutectic Alloy	22
9.	The Effect of Rotational Speed of the Disc on the Maximum Dissolution Flux of Iron from 304 SS at 860°C	23
10.	The Effect of Rotational Speed of the Disc on the Maximum Dissolution Flux of 304 SS at 860°C	23
11.	The Temperature Dependence of the Maximum Dissolution Flux of Iron at 10.0 rpm	24
12.	The Temperature Dependence of the Maximum Dissolution Flux of 304 SS at 10.0 rpm	24
13.	Micrographs of the Cross Section and Surface of a Disc Sample at the Conclusion of a 150-hr Dissolution Run at 860°C	27

LIST OF TABLES

No.	Title	Page
I.	Values of the Integral $I_{(D/\nu)}$ for a Range of Schmidt Numbers between 4 and 1000	16
II.	Values for the Hydrodynamic and Convective-diffusion Boundary Layers Produced by a 5.08-cm-diam Disc Rotating in the Bismuth-Tin Eutectic Alloy at 860°C	18
III.	Viscosity Data for the Bismuth-Tin Eutectic Alloy	18
IV.	Slopes of the Initial Portion of the Concentration-vs-Time Curves for Iron and the Maximum Flux of Iron, $J_m(Fe)$, from 304 SS into the Bismuth-Tin Eutectic Alloy with 60% Confidence Limits	23

A CONVECTIVE-DIFFUSION STUDY OF THE DISSOLUTION KINETICS OF 304 STAINLESS STEEL IN THE BISMUTH-TIN EUTECTIC ALLOY

by

T. F. Kassner

ABSTRACT

The kinetics of dissolution of Type 304 stainless steel in the bismuth-42w/o tin eutectic alloy have been investigated under the well-defined hydrodynamic conditions produced by the rotating-disc sample geometry. The experiments were carried out in the temperature interval of 200 to 1100°C at rotational speeds between 2 and 150 rpm. A convective-diffusion model was used to interpret the experimental data. The dissolution process was found to be liquid-diffusion controlled under specific conditions of temperature and Reynolds number.

INTRODUCTION

The use of liquid metals in nuclear reactor designs as heat-transfer fluids, as fuel dispersants, and as fusible sealants in certain reactors has necessitated the investigation of numerous problems of corrosion and mass transport inherent in liquid-metal systems. Most of the experimental work in the area of liquid-metal corrosion is undertaken with the immediate objective of finding the most suitable container or fuel cladding material. Static capsule tests and dynamic tests involving both thermal-convection and forced-circulation loops have become almost universal standards for determining the relative corrosion behavior of materials. In comparison, relatively little has been done to investigate the basic mechanisms by which corrosion takes place. The result of the wide imbalance in effort between fundamental studies and engineering tests has been to reduce the effectiveness of the engineering tests from the standpoint of being able to extrapolate the data with confidence to reactor systems having varying environmental conditions. The present investigation was undertaken with the following objectives: 1) to investigate a liquid-metal corrosion process in a manner permitting a quantitative treatment of mass transport; 2) to evaluate the potential corrosion problem of Type 304 stainless steel used as the containment material for the low-melting, bismuth-tin eutectic alloy in the EBR-II reactor seal.

KINETICS OF DISSOLUTION

The theoretical basis for the kinetics of dissolution of solids in liquids has been formulated from numerous studies of the solution of inorganic and organic salts in water and in nonaqueous solvents. Bircumshaw and Riddiford[1] have reviewed much of this work. Dissolution data for solid metals in liquid metals have also been interpreted in terms of the general framework developed for the aqueous systems.[2-5]

The overall dissolution rate of a solid in a liquid is determined by the relative magnitudes of the rate at which atoms pass from the solid surface into the liquid layer immediately adjacent to the solid, and the rate at which the atoms diffuse from the liquid layer into the bulk of the liquid bath.

The Nernst-Brunner equation,[6] which defines the rate of flow of atoms across an area A into a volume V*, can be written as

$$\frac{dC}{dt} = \frac{KA}{V^*}(C_s - C), \tag{1}$$

where C_s is the saturation concentration of solute in the liquid phase and C is the concentration at any time, t. The proportionality constant K is the solution rate constant for the dissolution process and can be written as

$$K = \frac{k_s k_d}{k_d + k_s} = \frac{k_s(D/\delta_N)}{(D/\delta_N) + k_s}, \tag{2}$$

where k_s is the rate constant for the passage of solute atoms into the diffusion layer, and $k_d = D/\delta_N$ is the rate constant for the diffusion of solute atoms across the boundary layer δ_N. When diffusion in the liquid is rate-controlling, $K = D/\delta_N$; when passage of solute atoms into the liquid is rate-controlling, $K = k_s$.

Nernst and Brunner originally postulated that interfacial reactions are fast enough to cause the overall reaction rate to be limited by the rate at which reactants can diffuse across an effectively stagnant film of thickness δ_N. Three important implications of this postulate, which can be seen from Equation (1), are: (1) the reaction kinetics should be first-order with respect to the bulk reactant concentration; (2) the temperature dependence of the observed reaction rate should be characteristic of a molecular diffusion process, and not that of a chemical reaction; and (3) the reaction rate should be influenced by stirring conditions through changes in the effective diffusion film, δ_N.

The Nernst-Brunner theory, when first proposed, was viewed as a general theory for heterogeneous reactions. In subsequent years, the theory encountered considerable criticism because it was found that dissolution in many systems was not influenced by hydrodynamic factors. Criticism was also directed at the oversimplification of the "stagnant-layer" concept and the fact that no means of calculating the effective diffusion layer was proposed. With regard to the first criticism, the theory was eventually recognized to be the limiting case for liquid-diffusion-controlled dissolution rates. The diffusion-controlled consequences of the theory have since been placed upon firm theoretical ground by Levich.[7,8] The quantitative treatment for mass transport in liquid is developed in the following section for the rotating-disc sample configuration used in this study.

CONVECTIVE DIFFUSION IN LIQUIDS

Two mechanisms are involved in the transport of a solute by a moving liquid. First, molecular diffusion results from concentration differences in the liquid; second, solute particles are entrained by the moving liquid and transported with it. The combination of these two processes is called convective diffusion of the solute in the liquid.

When a reaction involving the solute takes place at a solid-liquid interface, the concentration of solute in the liquid phase may vary from point to point in the liquid as a function of time. The differential equation that is satisfied by the function $C(x,y,z,t)$ in a moving liquid can be written as

$$J_{Total} = J_{Diffusion} + J_{Convection}$$

or

$$J_{Total} = -D \text{ grad } C + CV. \tag{3}$$

The first term on the right represents the diffusional flux of solute under a concentration gradient, and the second term gives the additional flux of solute that is entrained by the flowing stream. Application of the continuity equation

$$\frac{\partial C}{\partial t} = -\text{div } J_T \tag{4}$$

to Equation (3), along with the assumptions that D, the solute diffusivity, is independent of composition and that the liquid is an incompressible fluid, yields the following general equation for convective diffusion of a solute in the liquid:

$$\frac{\partial C}{\partial t} = D\nabla^2 C - V \text{ grad } C. \tag{5}$$

In the cylindrical-coordinate system, Equation (5) becomes

$$\frac{\partial C}{\partial t} = D\left[\frac{\partial^2 C}{\partial y^2} + \frac{\partial^2 C}{\partial r^2} + \frac{1}{r}\frac{\partial C}{\partial r} + \frac{1}{r^2}\frac{\partial^2 C}{\partial \phi^2}\right] - \left[V_r \frac{\partial C}{\partial r} + \frac{V\phi}{r}\frac{\partial C}{\partial r} + V_y \frac{\partial C}{\partial y}\right]. \quad (6)$$

The first group of terms on the right represents the unsteady-state diffusion of solute (Fick's Second Law). The other terms take into account the effect of fluid motion on the distribution of solute in the liquid phase. The factors V_r, $V\phi$, and V_y are the velocity components of fluid flow in the radial, tangential, and axial directions, respectively, and are a function of position within the system.

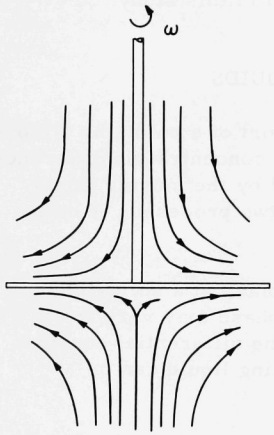

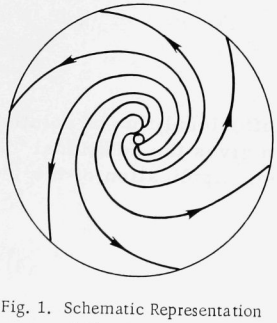

Fig. 1. Schematic Representation of Flow Lines near the Surface of a Rotating Disc

A mathematical solution to Equation (6) can be obtained by specifying a sufficient number of boundary and initial conditions if the velocity functions V_r, $V\phi$, and V_y are known. The boundary and initial conditions depend upon the nature of the physiochemical processes in which the solute takes part. The velocity functions are dependent upon the geometrical configuration of the system in which the processes occur and the physical properties of the liquid phase.

Unfortunately, there are very few flow systems in which the velocity distributions through the main body of the fluid are known. Cochran[9] and von Karman,[10] however, have been able to solve the Navier-Stokes hydrodynamic equations for the geometrical configuration of a thin disc rotating in a large volume of liquid to yield the desired velocity distributions.

A qualitative picture of fluid flow in a rotating disc system is shown in Fig. 1. Far from the disc, the fluid moves toward the disc, and in the thin layer immediately adjacent to the disc surface, the fluid acquires a rotating motion. The angular velocity of the fluid increases as the surface of the disc is approached, until the angular velocity of the rotating disc is attained. The fluid also acquires a radial velocity under the influence of the centrifugal force.

Cochran's[9] solution to the Navier-Stokes and continuity equations in cylindrical coordinates has the following form:

$$V_r = r\omega F(\xi), \quad V_\phi = r\omega G(\xi), \quad V_y = (\nu\omega)^{1/2} H(\xi).$$

The independent variable, ξ, is defined as

$$\xi = (\omega/\nu)^{1/2} y, \tag{7}$$

where ω is the angular velocity of the disc in rad/sec, r is the radius of the disc in cm, y is the axial distance from the disc in cm, and ν is the kinematic viscosity of the liquid in cm^2/sec. The functions $F(\xi)$, $G(\xi)$, and $H(\xi)$ taken from Cochran's paper are shown in Fig. 2.

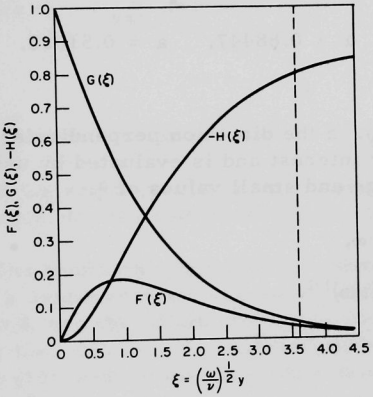

Fig. 2

Graph of the Functions $F(\xi)$, $G(\xi)$, and $-H(\xi)$ (from Cochran[9])

The analytical expressions that represent the functions in Fig. 2 are given below for both large [Equations (8) to (10)] and small [Equations (11) to (13)] values of the distance coordinate, ξ.

For large values of ξ,

$$F(\xi) = A\, e^{-\alpha\xi} - \frac{A^2 + B^2}{2\alpha^2}\, e^{-2\alpha\xi} + \frac{A(A^2+B^2)}{4\alpha^4}\, e^{-3\alpha\xi} + \ldots, \tag{8}$$

$$G(\xi) = B^{-\alpha\xi} - \frac{B(A^2+B^2)}{12\alpha^4}\, e^{-3\alpha\xi} + \ldots, \tag{9}$$

and

$$H(\xi) = -\alpha + \frac{2A}{\alpha}\, e^{-\alpha\xi} - \frac{A^2 + B^2}{2\alpha^3}\, e^{-2\alpha\xi} + \ldots . \tag{10}$$

For small values of ξ,

$$F(\xi) = a\xi - \tfrac{1}{2}\xi^2 - \tfrac{1}{3}b\xi^3 + \ldots, \tag{11}$$

$$G(\xi) = 1 + b\xi + \tfrac{1}{3}\alpha\xi^3 + \ldots, \tag{12}$$

and

$$H(\xi) = -a\xi^2 + \tfrac{1}{3}\xi^3 + \tfrac{1}{6}b\xi^4 + \tfrac{1}{30}b^2\xi^5 + \ldots . \tag{13}$$

The values of the constants in Equations (8) to (13) were obtained from Cochran[9] and Sparrow and Gregg[11] and are as follows:

$A = 0.934$, $B = 1.208$, $\alpha = 0.88447$, $a = 0.51023$,

and $b = -0.616$.

The velocity component, V_y, in the direction perpendicular to the surface of the disc is of particular interest and is evaluated by using the appropriate constants for both large and small values of ξ.

For large values of ξ, $y \to \infty$,

$$V_y = -\alpha(\nu\omega)^{1/2} = -0.88447(\nu\omega)^{1/2}. \tag{14}$$

For small values of ξ; $y \ll (\nu/\omega)^{1/2}$,

$$V_y = -a\xi^2(\nu\omega)^{1/2} + \tfrac{1}{3}\xi^3(\nu\omega)^{1/2} + \tfrac{1}{6}b\xi^4(\nu\omega)^{1/2},$$

or

$$V_y = -0.510\left(\frac{\omega^3}{\nu}\right)^{1/2} y^2 + 0.333\left(\frac{\omega^2}{\nu}\right) y^3 - 0.103\omega^{5/2}\nu^{-3/2}y^4. \tag{15}$$

Only the first term in Equation (10) was used to obtain V_y in Equation (14) for large values of ξ.

A definition of the hydrodynamic boundary layer can also be obtained from Equation (7) and the curves shown in Fig. 2. The hydrodynamic boundary layer is the thickness of the region across which the principal change in velocity occurs. Since the curves in Fig. 2 are continuous functions of distance, the definition of the boundary-layer thickness is somewhat arbitrary. Figure 2 indicates that the principal change in the velocity components occurs when ξ increases from 0 to a value around 3.5. If one chooses a ξ value of 3.6, the velocity component V_y, curve $H(\xi)$, has reached 80% of its

limiting value. The tangential component V_ϕ, curve $G(\xi)$, is 6% of the value at the surface of the disc, or has undergone a 94% change. For values of ξ greater than 3.6, the values of the velocity components change gradually. Thus, if a value of 3.6 is used for ξ in Equation (7), the hydrodynamic boundary layer becomes

$$y_h = \delta_h = 3.6(\nu/\omega)^{1/2}. \tag{16}$$

The boundary and initial conditions for a thin disc undergoing dissolution in a large volume of liquid are as follows:

$$C(y,t) = C_B \text{ as } y \to \infty, \tag{17}$$

$$C(y,t) = C_{sat.} \text{ at } y = 0, \tag{18}$$

and

$$\frac{\partial C}{\partial t}(y,t) = 0 \text{ for } t = 0. \tag{19}$$

$C_{sat.}$ and C_B are the equilibrium solubility and initial solute concentration, respectively, for the individual solute species in the liquid.

The boundary conditions set forth in Equations (17) and (18) are those of a unidimensional transport problem. Axial symmetry is assumed, $\partial C/\partial \phi = 0$, and the solute concentration is taken to be independent of radial position; i.e., $\partial C/\partial r = 0$. These assumptions, plus the initial condition in Equation (19), reduce the convective diffusion equation to the following form:

$$V_y \frac{\partial C}{\partial y} = D \frac{\partial^2 C}{\partial y^2}. \tag{20}$$

Equation (20) can be integrated twice, and the constants of integration can be evaluated from the boundary conditions. The first integration of Equation (20) gives

$$\frac{dC}{dy} = a_1 \exp\left[\frac{1}{D}\int_0^y V_y(z)\, dz\right]. \tag{21}$$

Integrating again, we obtain

$$C = a_1 \int_0^y \exp\left[\frac{1}{D}\int_0^t V_y(z)\, dz\right] dt + a_2. \tag{22}$$

By applying the boundary condition in Equation (18), $C = C_{sat.}$ at $y = 0$, the constant a_2 becomes $C_{sat.}$.

The constant a_1 can be determined from the boundary condition in Equation (17), $C = C_B$ as $y \to \infty$. Equation (22) can be written as

$$C_B - C_{sat.} = a_1 \int_0^{\infty} \exp\left[\frac{1}{D}\int_0^t V_y(z)\,dz\right] dt. \tag{23}$$

The integral can be evaluated by the following procedure. The integral is first divided into two regions; from $y = 0$ to $y = \delta_h$, and from $y = \delta_h$ to $y = \infty$. The values for the functions $V_y(z)$ for the two regions, defined by Equations (15) and (14), respectively, have been substituted into the respective integrals. The result is

$$C_B - C_{sat.} = a_1 \int_0^{\delta_h} \exp\left\{\frac{1}{D}\int_0^t \left[-0.510\left(\frac{\omega^3}{\nu}\right)^{1/2} z^2 + 0.333\left(\frac{\omega^2}{\nu}\right) z^3 - 0.103\omega^{5/2}\nu^{-3/2} z^4\right] dz\right\} dt$$

$$+ a_1 \int_{\delta_h}^{\infty} \exp\left[\frac{1}{D}\int_0^t -0.89(\nu\omega)^{1/2}\,dz\right] dt. \tag{24}$$

By integrating Equation (24) with respect to z, we obtain

$$C_B - C_{sat.} = a_1 \int_0^{\delta_h} \exp\left[-\frac{0.17}{D}\left(\frac{\omega^3}{\nu}\right)^{1/2} t^3 + \frac{0.0833}{D}\left(\frac{\omega^2}{\nu}\right) t^4 - 0.0206\omega^{5/2}\nu^{-3/2} t^5\right] dt$$

$$+ a_1 \int_{\delta_h}^{\infty} \exp\left[-\frac{0.89}{D}(\nu\omega)^{1/2} t\right] dt. \tag{25}$$

The two integrals in Equation (25) are evaluated separately. The first integral can be simplified by making the following substitutions.

When $X^3 = (0.17/D)(\omega^3/\nu)^{1/2} t^3$, then $t = (1.805\omega^{-1/2}\nu^{1/6}D^{1/3})\,X$, and the first integral can be rewritten as

$$1.805 a_1 \omega^{-1/2}\nu^{1/6}D^{1/3} \int_0^{X_h} \exp\left[-X^3 + 0.885\left(\frac{D}{\nu}\right)^{1/3} X^4 - 0.394\left(\frac{D}{\nu}\right)^{2/3} X^5\right] dX.$$

The new limit of integration, X_h, is evaluated as

$$X_h = \frac{t_h}{1.805\omega^{-1/2}\nu^{1/6}D^{1/3}},$$

where

$$t_h = \delta_h = 3.6\left(\frac{\nu}{\omega}\right)^{1/2},$$

or

$$X_h = 1.9944\left(\frac{\nu}{D}\right)^{1/3},$$

The second integral in Equation (25) can be integrated directly to give

$$-\frac{a_1 D}{0.89(\nu\omega)^{1/2}} \exp\left[-\frac{0.89(\nu\omega)^{1/2}}{D}\right] t \Bigg|_{\delta_h}^{\infty},$$

and when the value of δ_h is inserted for the lower limit, we get

$$+\frac{a_1 D}{0.89(\nu\omega)^{1/2}} \exp\left[-3.11\left(\frac{\nu}{D}\right)\right].$$

Equation (25) can now be rewritten as

$$C_B - C_{sat.} = 1.805 a_1 \omega^{-1/2} \nu^{1/6} D^{1/3} \int_0^{1.9944\left(\frac{\nu}{D}\right)^{1/3}} \exp\left[-X^3 + 0.885\left(\frac{D}{\nu}\right)^{1/3} X^4 - 0.394\left(\frac{D}{\nu}\right)^{2/3} X^5\right] dX$$

$$+ 1.124 a_1 (\nu\omega)^{-1/2} D \exp\left[-3.11\left(\frac{\nu}{D}\right)\right], \qquad (26)$$

and the constant a_1 becomes

$$a_1 = \frac{C_B - C_{sat.}}{1.805\omega^{-1/2}\nu^{1/6}D^{1/3} I\left(\frac{D}{\nu}\right) + 1.124 D(\nu\omega)^{-1/2} \exp\left[-3.11\left(\frac{\nu}{D}\right)\right]}$$

where the integral in Equation (26) is represented by $I_{(D/\nu)}$.

Numerical values for the integral in Equation (26) have been obtained for a series of values for D/ν between 0.001 and 0.25 by the use of digital-computer methods. Gregory and Riddiford[12] have computed $I_{(D/\nu)}$ graphically by using the X^3 and X^4 terms for several values of D/ν in the range 0 to 0.004. This range is applicable to aqueous solutions near ambient temperatures. Since D/ν values as large as 0.25 cm can be encountered in liquid-metal systems at high temperatures, the integral was evaluated over the entire range by using three terms. The results are shown in Table I. Gregory and Riddiford have shown that when $D/\nu = 10^{-3}$, $I_{(D/\nu)}$ is 3% less than the value at $I_{(0)}$ used by Levich.[7] Table I shows that when $D/\nu = 0.1$, a value applicable in this work, $I_{(D/\nu)}$ is 16% less than the value obtained with the approximation $D/\nu \approx 0$.

TABLE I. Values of the Integral $I_{(D/\nu)}$ for a Range of Schmidt Numbers between 4 and 1000

$(\text{Schmidt No.})^{-1}$, D/ν	Integration Limit, $1.9944(\nu/D)^{1/3}$	Value of the Integral, $I_{(D/\nu)}$
0	∞	0.8934
0.001	19.944	0.9209
0.002	15.830	0.9286
0.003	13.828	0.9341
0.004	12.564	0.9385
0.005	11.663	0.9424
0.006	10.976	0.9457
0.007	10.426	0.9487
0.008	9.972	0.9515
0.009	9.588	0.9541
0.010	9.257	0.9564
0.020	7.347	0.9747
0.030	6.419	0.9877
0.040	5.832	0.9981
0.050	5.414	1.0068
0.060	5.094	1.0143
0.070	4.839	1.0209
0.080	4.629	1.0268
0.090	4.450	1.0321
0.100	4.297	1.0368
0.110	4.162	1.0412
0.120	4.043	1.0451
0.130	3.937	1.0488
0.140	3.841	1.0521
0.150	3.754	1.0552
0.160	3.674	1.0580
0.180	3.532	1.0631
0.200	3.410	1.0675
0.250	3.166	1.0762

The value of the constant a_1 can now be substituted into Equation (22) to give the concentration distribution of solute near the surface of the disc, as follows:

$$\frac{C - C_{sat.}}{C_B - C_{sat.}} = \frac{\int_0^y \exp\left[\frac{1}{D}\int_0^t V_y(z)\,dz\right] dt}{1.805\omega^{-1/2}\nu^{1/6}D^{1/3}I_{(D/\nu)} + 1.124D(\nu\omega)^{-1/2}\exp\left[-3.11\left(\frac{\nu}{D}\right)\right]}. \quad (27)$$

To obtain the mass flux of material away from the surface of the disc, Equation (27) is first differentiated with respect to y and evaluated at y = 0. The value of $V_y(z)$ for the region y = 0 to y = δ_h is substituted into the equation before the integral is evaluated. The result is

$$\frac{\partial C}{\partial y} = \frac{(C_B - C_{sat.})\exp\left[-\frac{0.17}{D}\left(\frac{\omega^3}{\nu}\right)^{1/2}y^3 + \frac{0.0833}{D}\left(\frac{\omega^2}{\nu}\right)y^4 - 0.0206\omega^{5/2}\nu^{-3/2}y^5\right]}{1.805\omega^{-1/2}\nu^{1/6}D^{1/3}I_{(D/\nu)} + 1.124D(\nu\omega)^{-1/2}\exp\left[-3.11\left(\frac{\nu}{D}\right)\right]} \quad (28)$$

$$\left.\frac{\partial C}{\partial y}\right)_{y=0} = \frac{C_B - C_{sat.}}{1.805\omega^{-1/2}\nu^{1/6}D^{1/3}I_{(D/\nu)} + 1.124D(\nu\omega)^{-1/2}\exp\left[-3.11\left(\frac{\nu}{D}\right)\right]}.$$

The above result, when substituted into Fick's First Law,

$$J_m = -D\left.\frac{\partial C}{\partial y}\right)_{y=0},$$

gives the mass flux of material away from the disc:

$$J_m = \frac{D(C_{sat.} - C_B)}{1.805\omega^{-1/2}\nu^{1/6}D^{1/3}I_{(D/\nu)} + 1.124D(\nu\omega)^{-1/2}\exp\left[-3.11\left(\frac{\nu}{D}\right)\right]}. \quad (29)$$

The convective diffusion boundary layer δ_D is defined by the denominator of Equation (29),

$$\delta_D = 1.805\omega^{-1/2}\nu^{1/6}D^{1/3}I_{(D/\nu)} + 1.124D(\nu\omega)^{-1/2}\exp\left[-3.11\left(\frac{\nu}{D}\right)\right]. \quad (30)$$

The equations developed above for the mass transport of a solute away from a rotating-disc sample apply only to laminar flow. The region of laminar flow for a polished and dynamically balanced disc extends to Reynolds numbers of the order of 10^5, where the Reynolds number is defined as

$$Re = \frac{\omega r^2}{\nu}. \tag{31}$$

The lower limit of the Reynolds number is determined by the relative magnitudes of the hydrodynamic boundary layer and the radius of the disc. At low rotational speeds, the hydrodynamic boundary layer approaches the radius of the disc in size; however, a rotational speed that produces a hydrodynamic boundary layer of about one-tenth the radius of the disc is more commonly used as a lower limit.

Values for the hydrodynamic and convective-diffusion boundary layers as a function of rotational speed of a 5.08-cm-diam disc in the bismuth-tin eutectic liquid at 860°C are shown in Table II. A credible solute diffusivity of 1×10^{-4} cm^2/sec was used, along with a kinematic viscosity value of 10.25×10^{-4} cm^2/sec extrapolated from Sauerwald and Toppler's[13] data in Table III, to obtain the values for the convective-diffusion boundary layer. For the above values of D and ν, D/ν is 0.10, and $I_{(D/\nu)}$ from Table I is 1.0368. Table II also gives the range of rotational speeds (2 to 150 rpm) applicable to the rotating disc-bismuth-tin system at 860°C.

TABLE II. Values for the Hydrodynamic and Convective-diffusion Boundary Layers Produced by a 5.08-cm-diam Disc Rotating in Bismuth-Tin Eutectic Alloy at 860°C

Speed, rpm	ω, rad/sec	$\omega^{1/2}$	ν/ω	δ_h, cm	δ_D, cm*	Reynolds No.
151.6	15.89	3.99	0.646×10^{-4}	2.89×10^{-2}	0.694×10^{-2}	1.00×10^{5}
150.0	15.70	3.96	0.653×10^{-4}	2.91×10^{-2}	0.700×10^{-2}	9.88×10^{4}
100.0	10.48	3.24	0.979×10^{-4}	3.56×10^{-2}	0.854×10^{-2}	6.59×10^{4}
50.0	5.29	2.30	1.940×10^{-4}	5.01×10^{-2}	1.203×10^{-2}	3.33×10^{4}
30.0	3.17	1.78	3.235×10^{-4}	6.48×10^{-2}	1.555×10^{-2}	2.00×10^{4}
10.0	1.048	1.025	9.790×10^{-4}	11.25×10^{-2}	2.699×10^{-2}	6.59×10^{3}
5.0	0.529	0.727	19.40×10^{-4}	15.85×10^{-2}	3.807×10^{-2}	3.33×10^{3}
2.0	0.2095	0.458	49.00×10^{-4}	25.20×10^{-2}	6.048×10^{-2}	1.32×10^{3}

*A solute diffusivity of 1.0×10^{-4} cm^2/sec was used in the calculation of the convective-diffusion boundary layer.

TABLE III. Viscosity Data for the Bismuth-Tin Eutectic Alloy[13]

Temp, °C	Viscosity, η, poise	Density, g/cm^3	Viscosity, ν, cm^2/sec
751	0.00886	8.100	10.95×10^{-4}
750	0.00898	8.100	11.09×10^{-4}
606	0.01014	8.245	12.30×10^{-4}
599	0.01029	8.245	12.47×10^{-4}
445	0.01257	8.385	15.00×10^{-4}
445	0.01267	8.385	15.11×10^{-4}
305	0.01690	8.520	19.85×10^{-4}

$$\nu = 5.30 \times 10^{-4} \exp\left(\frac{756}{T°K}\right), \qquad \nu_{860°C} = 10.25 \times 10^{-4} \text{ cm}^2/\text{sec}$$

EXPERIMENTAL METHOD

The Bi-42w/oSn eutectic alloy used in each run was prepared from 99.995% pure bismuth and tin by fusing desired weights of the two components in a 7.0-cm-ID Pyrex crucible. The system in which the melt was made was evacuated to a pressure of 1×10^{-6} Torr and backfilled with purified argon several times before melting the charge. The eutectic liquid was held at 300°C under a dynamic vacuum of 1×10^{-6} Torr for about 10 hr prior to solidification. The resulting ingot was reweighed and then placed in a slightly larger-diameter Vycor crucible used in the dissolution runs.

Type 304 stainless-steel discs 5.08 cm in diameter were machined from 0.317-cm-thick plate. Chemical-analysis information for the 304 SS material is given in Appendix A. After the discs were drilled and tapped to accept the threaded support rod, the discs were abraded through Grade 600A metallographic paper. The final polishing was done on Linde B abrasive. A polished disc was threaded into a support rod, and the region around the threads was fused with a Heliarc welder. The disc and supporting shafts were dynamically balanced in a lathe and then tested in the apparatus to insure that the disc ran true.

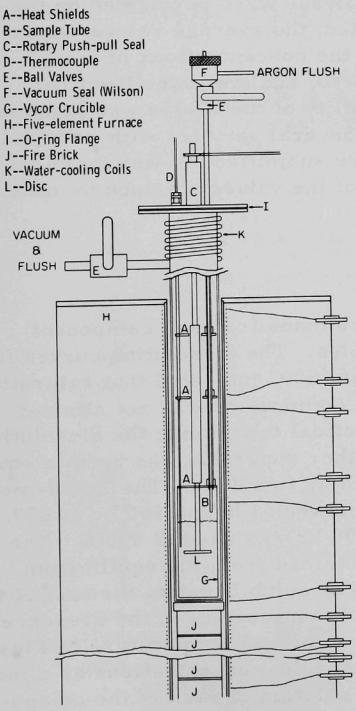

Fig. 3. Schematic Diagram of the Dissolution Apparatus

The apparatus in which the dissolution runs were made is shown schematically in Fig. 3. While the system was heating to the desired temperature, the disc was positioned 5 cm above the liquid bath. A dissolution run was started by lowering the disc into the bath by means of a rotary, push-pull, vacuum seal. The rotational speed of the disc was set and maintained at a constant speed by an electronically controlled motor. The rotational speed was controlled to ±1% of the set value, and the temperature of the bath was held to ±1°C. Vertical temperature profiles within the liquid bath indicated a 5°C variation over the length, the majority of which occurred near the liquid-gas interface. A slight positive pressure of purified argon was maintained in the system during a dissolution run to suppress the loss of liquid metal from the crucible by vaporization and condensation in colder parts of the

system. Liquid-metal samples weighing from 4 to 5 g were obtained from the bath at desired time intervals during the run by using Vycor sampling tubes.

The samples were analyzed spectrographically for iron, chromium, nickel, and manganese by the following method. The bismuth-tin samples were drilled at several points along the length of the sample to minimize any effects of segregation during solidification. A representative portion of the drillings (~50 to 100 mg) were digested in 90:10 HCl-HNO_3 acid solution. Aliquots of the solution were quantitatively pipetted onto the surface of spectrographic electrodes. Silver electrodes were used in obtaining the analysis results for iron, chromium, and nickel. Copper electrodes were used in the manganese analyses to achieve a lower manganese background.

The samples were excited using an a.c. arc method. The line intensities were determined with a densitometer and then compared with intensities obtained from bismith-tin standard solutions prepared with known amounts of the four elements. Duplicate analyses were performed on the majority of the bismuth-tin samples submitted; the average values are reported in Appendix B. The lower limits for the concentrations of iron, chromium, and nickel were routinely 0.005 w/o, and the lower limit for manganese was 0.0005 w/o. The reproducibility of the values was found to be better than ±10% of the amount present. Several samples with relatively high concentrations of the four elements were submitted for wet chemical analysis, and the results agreed within ±3% of the values obtained by means of the spectrographic method.

RESULTS

Concentration-versus-time plots were made for each component undergoing dissolution from the 304 SS samples. The dissolution curves for chromium, nickel, and manganese obtained at 650°C indicated that saturation of the liquid bath with respect to these three components was not attained during the first 100 hr. Since it was not practical to continue the dissolution runs for times much longer than 100 hr, another apparatus was used to equilibrate 304 SS with the eutectic alloy for times up to 500 hr. The liquid-metal bath was sampled at several time intervals between 100 and 500 hr at 450, 650, and 860°C. An equilibration period of 190 hr was used at 985°C. The chemical-analysis results for the samples obtained from the equilibrium solubility run are tabulated in Appendix C. The solubility data for each of the four components (iron, chromium, nickel, and manganese), in the presence of the other three, are plotted as a function of reciprocal temperature in Figs. 4 to 7, respectively. Least-squares equations for the concentrations as a function of temperature, and the overall heats of solution of each of the components, are shown on the plots with 95% confidence limits. Three solubility values listed in Appendix C for manganese at 450°C were included in the calculations of the least-squares line in Fig. 7. The temperature dependence of the solubility of 304 SS in the Bi-42w/oSn alloy in Fig. 8 was obtained by summing the results shown in Figs. 4 to 7.

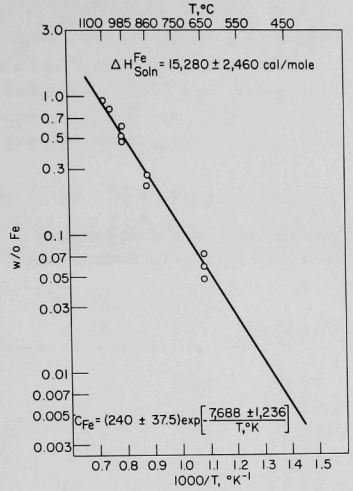

Fig. 4. Temperature Dependence of the Solubility of Iron from 304 SS in the Bismuth-Tin Eutectic Alloy

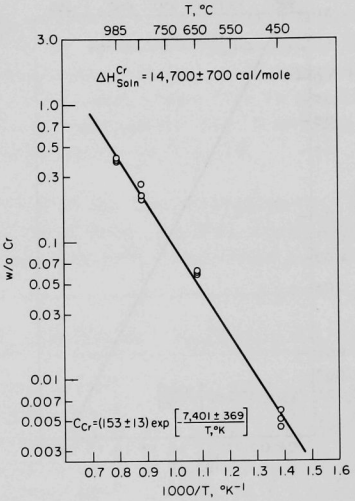

Fig. 5. Temperature Dependence of the Solubility of Chromium from 304 SS in the Bismuth-Tin Eutectic Alloy

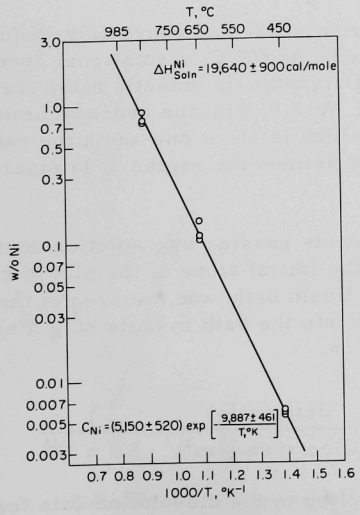

Fig. 6. Temperature Dependence of the Solubility of Nickel from 304 SS in the Bismuth-Tin Eutectic Alloy

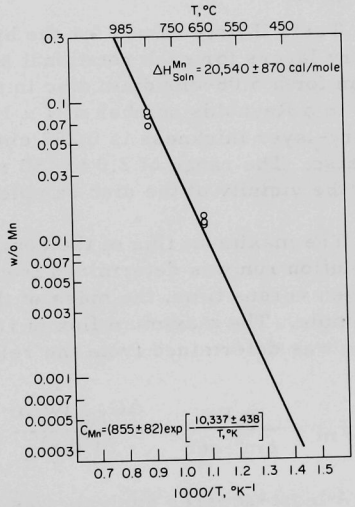

Fig. 7. Temperature Dependence of the Solubility of Manganese from 304 SS in the Bismuth-Tin Eutectic Alloy

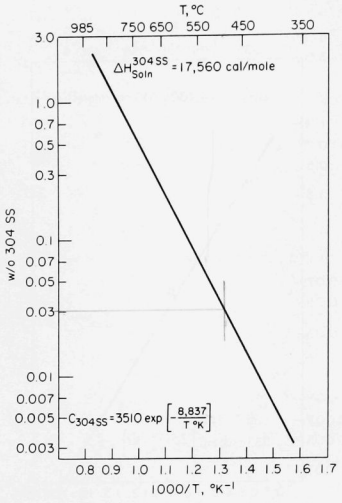

Fig. 8

Temperature Dependence of the Solubility of 304 SS in the Bismuth-Tin Eutectic Alloy

The investigation of the effect of the rotational speed of the disc was carried out at 860°C, a temperature at which the concentrations of all of the elements could be determined at times greater than 0.5 hr. At this temperature, dissolution runs were made at 2, 10, 30, 50, 100, and 150 rpm for times up to 150 hr.

Table II lists values for the hydrodynamic and convective-diffusion boundary layers for each rotational speed. At 860°C, a rotational speed of 150 rpm for a 5.08-cm-diam disc in the bismuth-tin eutectic alloy corresponds to a Reynolds number of 1×10^5. At 2.0 rpm, the hydrodynamic boundary-layer thickness is 0.252 cm, which is about one-tenth the radius of the disc. The range of 2.0 to 150 rpm defines the region of laminar flow in the vicinity of the disc sample.

The maximum flux of the components passing into solution during a dissolution run was determined from the initial slope of the plot of concentration versus time, the mass of the liquid bath, and the area of the disc sample. The maximum flux of iron into the bath in units of g Fe/cm^2-sec was determined from the relation,

$$J_m = \frac{\text{g Fe}}{\text{cm}^2\text{-sec}} = \frac{\Delta C_{Fe}\ (\text{w/o})}{\Delta t\ (\text{hr})} \cdot \frac{\text{Bath wt (g)}}{\text{Disc area (cm}^2)} \cdot \frac{1}{3.6 \times 10^5}. \qquad (32)$$

A least-squares analysis was applied to the dissolution data for iron tabulated in Appendix B to obtain values of $(\Delta C_{Fe}\ \text{w/o})/(\Delta t\ \text{hr})$ for ten of the dissolution runs. The results are given in Table IV, along with

the values for the maximum flux of iron from 304 SS into the eutectic liquid. In Fig. 9, the values for the flux of iron at 860°C are plotted as a function of the square root of the angular velocity of the disc. Curves similar to the one in Fig. 9 can also be obtained for chromium, nickel, and manganese. Since iron was the largest contributor to the total mass flux in the dissolution experiments, the data can best be summarized by Fig. 9 and the total mass flux for the components from 304 SS shown in Fig. 10.

TABLE IV. Slopes of the Initial Portion of the Concentration-vs-Time Curves for Iron and the Maximum Flux of Iron, $J_m(Fe)$, from 304 SS into the Bismuth-Tin Eutectic Alloy with 60% Confidence Limits

Run No.	Speed, rpm	Temp, °C	Initial Slope, w/o Fe/hr	$J_m(Fe)$, g Fe/cm^2-sec
8	2.0	860	$(0.91 \pm 0.038) \times 10^{-2}$	$(2.50 \pm 0.10) \times 10^{-6}$
6	10.0	860	$(2.38 \pm 0.180) \times 10^{-2}$	$(6.53 \pm 0.40) \times 10^{-6}$
9 & 11	30.0	860	$(3.32 \pm 0.868) \times 10^{-2}$	$(9.15 \pm 2.40) \times 10^{-6}$
13	50.0	860	$(3.56 \pm 0.433) \times 10^{-2}$	$(9.92 \pm 1.19) \times 10^{-6}$
2	100.0	860	$(3.62 \pm 0.602) \times 10^{-2}$	$(9.98 \pm 1.66) \times 10^{-6}$
10	150.0	860	$(3.78 \pm 0.330) \times 10^{-2}$	$(10.40 \pm 0.91) \times 10^{-6}$
7	10	750	$(1.11 \pm 0.281) \times 10^{-2}$	$(3.05 \pm 0.77) \times 10^{-6}$
17	10	1050	$(3.36 \pm 0.232) \times 10^{-1}$	$(5.56 \pm 0.38) \times 10^{-5}$
16	10	1100	$(2.12 \pm 0.046) \times 10^{-1}$	$(3.50 \pm 0.08) \times 10^{-5}$

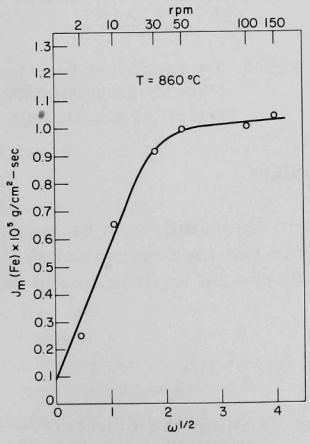

Fig. 9. The Effect of Rotational Speed of the Disc on the Maximum Dissolution Flux of Iron from 304 SS at 860°C

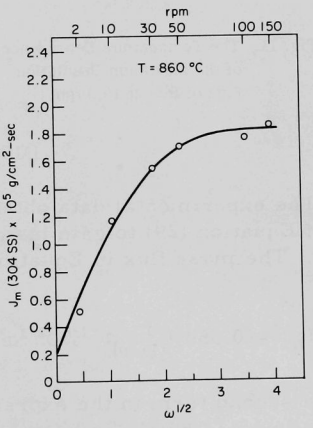

Fig. 10. The Effect of Rotational Speed of the Disc on the Maximum Dissolution Flux of 304 SS at 860°C

Dissolution runs were made at 750, 860, 1050, and 1100°C at a rotational speed of 10.0 rpm to investigate the temperature dependence of the dissolution process. Temperatures above 860°C were investigated because the concentration of the elements in the liquid were below the limits of detectability during the initial portion of the dissolution run at temperatures below 750°C. The maximum flux of iron for the runs at 10.0 rpm also appear in Table IV, and the values plotted versus reciprocal temperature are shown in Fig. 11. The activation energy of J_m(Fe) is 19,400 cal/mole for the temperature range of 750 to 1100°C. The activation energy of J_m(304 SS) determined from Fig. 12 is 18,800 cal/mole.

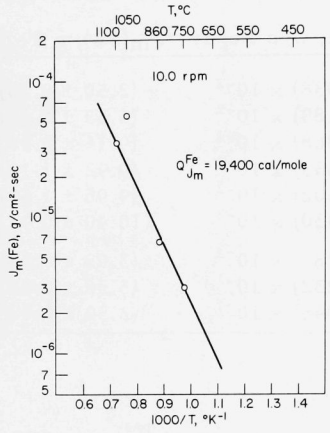

Fig. 11. The Temperature Dependence of the Maximum Dissolution Flux of Iron at 10.0 rpm

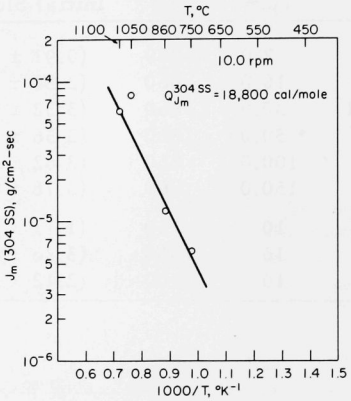

Fig. 12. The Temperature Dependence of the Maximum Dissolution Flux of 304 SS at 10.0 rpm

DISCUSSION

The experimental data obtained in this study can be analyzed in terms of Equation (29) to gain insight into the mechanism of the dissolution process. The mass flux in Equation (29) can be written in the following form:

$$J_m = 0.554\, I^{-1}_{(D/\nu)} \nu^{-1/6} D^{2/3} \omega^{1/2} (C_{sat.} - C_B), \qquad (33)$$

since the second term in the expression defining the convective-diffusion boundary layer is small, in comparison with the first. Equation (33) indicates that flux will vary with the half-power of the angular velocity of the disc for a liquid-diffusion-controlled process. Within the limits of the experimental errors, the data in Figs. 9 and 10 agree with the velocity

dependence predicted by the model for rotational speeds between 2 and 30 rpm. Above 50 rpm at 860°C, the maximum flux is no longer limited by diffusional processes in the liquid phase but is now dependent upon the mass-transfer rate at the solid-liquid interface.

The temperature dependence of J_m can be obtained by substituting the appropriate expressions for the temperature dependence of D, ν, and $C_{sat.}$ into Equation (33). When the relations

$$D = D_0 \exp(-Q_D/RT),\ \nu = \nu_0 \exp(+Q_\nu/RT), \text{ and } C_{sat.} = C_0 \exp(-\Delta H_{soln}/RT)$$

are inserted into Equation (33) with $C_B = 0$ (i.e., the solute concentration of the bath was zero at the start of the dissolution runs), the result is

$$J_m = 0.554\, I^{-1}_{(D/\nu)}\, D_0^{2/3}\, \nu_0^{-1/6}\, C_0 \omega^{1/2} \exp\left(-\frac{4Q_D + Q_\nu + 6\Delta H_{soln}}{6RT}\right). \qquad (34)$$

The temperature dependence of the flux, Q_{J_m}, is related to the overall heat of solution of the solute in the liquid (ΔH_{soln}), the activation energies for the kinematic viscosity (Q_ν), and the solute diffusivity (Q_D) by the relation

$$Q_{J_m} = \tfrac{1}{6}(4Q_D + Q_\nu + 6\Delta H_{soln}). \qquad (35)$$

All the quantities in Equation (35) are known with the exception of the values of Q_D for the four components (Fe, Cr, Ni, and Mn) in the bismuth-tin eutectic alloy. A value of Q_D can be determined for the diffusivity of iron and for the "average" diffusivity of the four components by using the values of $Q^{Fe}_{J_m}$ and $Q^{304SS}_{J_m}$ from Figs. 11 and 12 and the heats of solution for iron and 304 SS from Figs. 4 and 8. A value of Q_ν of 1,500 cal/mole was obtained from the data in Table III. The activation energy for the diffusivity of iron in the bismuth-tin eutectic obtained from Equation (35) is 5,810 cal/mole, and the average value for the four components in 304 SS is 1,490 cal/mole. Measured activation energies for self and chemical diffusion in liquid-metal systems have been found to range between 1,000 and 9,700 cal/mole.[14-16] The fact that the value of Q_D for iron lies within this range is evidence for liquid-diffusion control of the dissolution process for the rotational speed of 10 rpm and the temperature range above ~700°C. Activation energies as high as 6,300 cal/mole have been reported for the solution rate constant obtained from the Nernst-Brunner equation for the copper-bismuth[2] and zinc-bismuth[5] systems. Liquid-diffusion-controlled dissolution was also postulated in the absence of experimental diffusion data.

A comparison of the values of J_m calculated from Equation (33) with experimental values obtained under conditions in which liquid-diffusion control is operative (i.e., below 30 rpm at 860°C) provides the final test of

the convective-diffusion model. When a D value for iron of 1×10^{-4} cm^2/sec is assumed for 860°C, the value of $J_m(Fe)$ at 10.0 rpm becomes 7.8×10^{-5} g Fe/cm^2-sec as compared to an experimental value of 0.65×10^{-5} g Fe/cm^2-sec (Run 6). Using a D value of 1×10^{-4} cm^2/sec leads to an order-of-magnitude difference between the predicted and observed dissolution fluxes. For a D value of 1×10^{-5} cm^2/sec, the calculated flux of iron is 1.83×10^{-5} cm^2/sec, or a factor of 2.8 greater than the experimental value.

Metallographic examination of the disc sample provides a qualitative explanation for the observed rates. Figures 13b and 13c show the cross section and the surface, respectively, of a disc sample at the conclusion of an 860°C dissolution run. Considerable penetration of the eutectic alloy into the 304 SS has occurred. Figure 13a shows that the penetration occurred uniformly from both sides of the disc. The depth of penetration was found to be independent of radial position on the disc. At temperatures of 750°C and higher, the recession of the solid interface was small and the disc retained its planar shape with no macroscopic surface roughening. The rotating disc sample can be considered to be a uniformly accessible surface from the standpoint of corrosion process at the higher temperatures.

Harrison and Wagner[17] have shown that rapid penetration of a solid by a liquid metal occurs when one component in an alloy is much more soluble than the other. Penetration of the 304 SS by the bismuth-tin eutectic alloy is not surprising since the solubility of nickel in the liquid (0.828 w/o at 860°C) is much greater than the solubility of either iron (0.269 w/o at 860°C) or chromium (0.222 w/o at 860°C). Also, the nickel content of 304 SS is less than 10% of the total constituents.

One result of liquid penetration into the disc sample is to decrease the effective area of solid in contact with the liquid at the plane of the solid-liquid interface. In addition, the material leaving the disc from the penetrated regions must diffuse through an additional path in the liquid before reaching the diffusion boundary layer at the surface of the disc. Both the reduction in surface area of the solid at the interface and the added diffusional length due to liquid penetration will decrease the mass flux from the sample.

The surface area of the disc may have been reduced by a factor of two or three from a comparison of the relative areas of the eutectic alloy and the 304 SS in Fig. 13c. The added diffusion length through the liquid cannot be estimated since the liquid did not penetrate perpendicular to the surface of the disc. The actual diffusion paths are longer than their projections shown in Fig. 13b. It would be difficult to relate these two effects quantitatively to the observed magnitude of the dissolution fluxes.

At temperatures of 650°C and lower, the dissolution process appears to be surface-reaction controlled. Only random areas of the disc sample were corroded. The mass flux of iron was independent of velocity at 650°C for rotational speeds of 10.0 and 100 rpm.

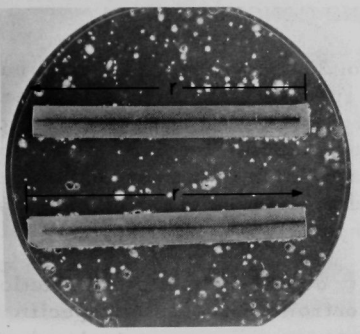

(a) Cross Section of the Disc Sample along a Diameter

41541 2X

41542 500X

(b) Cross Section near the Liquid-Solid Interface

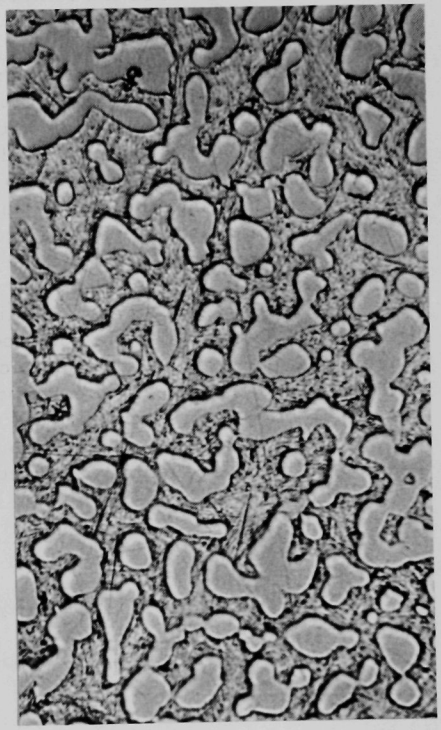

41543 500X

(c) Disc Surface

Fig. 13. Micrographs of the Cross Section and Surface of a Disc Sample at the Conclusion of a 150-hr Dissolution Run at 860°C. The region along the midplane of the disc is the unaffected material. The islands in b and c are "304 SS," the matrix is the bismuth-tin eutectic alloy.

SUMMARY AND CONCLUSIONS

The kinetics of dissolution of 304 SS in the Bi-42w/oSn eutectic alloy have been investigated under specified conditions of temperature and rotational speed for a system incorporating a rotating-disc-sample geometry. A mathematical description of the hydrodynamic conditions for the rotating-disc system was used in obtaining a solution to the convective-diffusion equation for mass transport. The experimental data were interpreted in terms of the convective-diffusion model.

The temperature and velocity dependence of the dissolution flux were consistent with a liquid-diffusion-controlled process for specific hydrodynamic conditions. A transition between diffusion control and reaction control was noted at 860°C by varying the rotation speed of the disc. The transition occurred when the temperature was decreased from 750 to 650°C at a rotational speed of 10.0 rpm.

Quantitative agreement was not attained between the magnitude of the mass flux obtained from the diffusion model and the experimental values. The effects of liquid penetration into the disc sample may account for the difference between the experimental and calculated diffusional fluxes. This point is under investigation in a two-component (liquid-solid) system where liquid penetration into the disc is unlikely. Solute diffusivity measurements in the liquid will also be made to provide a quantitative correlation for both the temperature dependence and the magnitude of the mass flux.

The use of 304 SS as a containment material for the low-melting, bismuth-tin eutectic alloy is not recommended at temperatures above 500°C. Since liquid penetration does not occur uniformly at the lower temperatures, average corrosion rates and equilibrium solubility data are not sufficient for specifying a minimum wall thickness for a containment vessel. At higher temperatures, the penetration of 304 SS by the eutectic alloy would result in a rapid weakening of structural parts.

APPENDIX A

Chemical Analysis for the 304 SS Sample Material

Element	Runs 1-6, w/o	Runs 7-13, w/o	Runs 14-17, w/o
Fe	70.10	70.10	70.44
Cr	18.13	18.25	18.65
Ni	9.72	9.38	9.03
Mn	1.29	2.24	1.80
C	0.04	0.04	0.07

APPENDIX B

Chemical-analysis Data for the Dissolution Runs

Run No. 1

T = 200°C, 150 rpm; Weight of Bi-Sn Bath = 4680 g; Weight of 304 SS Disc = 48.1472 g; Diam of Disc = 5.08 cm

Time, hr	Bi-Sn Bath Composition				ΣC_i,*
	w/o Fe	w/o Cr	w/o Ni	w/o Mn	w/o 304 SS
0	<0.005	<0.005	<0.001	<0.0005	~0
0.25	<0.005	<0.005	<0.001	<0.0005	~0
0.50	<0.005	<0.005	<0.001	<0.0005	~0
1.00	<0.005	<0.005	<0.001	<0.0005	~0
1.67	<0.005	<0.005	<0.001	<0.0005	~0
2.50	<0.005	<0.005	<0.001	<0.0005	~0
3.33	<0.005	<0.005	<0.001	<0.0005	~0
18.3	<0.005	<0.005	<0.001	<0.0005	~0
21.7	<0.005	<0.005	<0.001	<0.0005	~0
25.0	<0.005	<0.005	<0.001	<0.0005	~0

Run No. 2

T = 860°C, 100 rpm; Weight of Bi-Sn Bath = 4496 g; Weight of 304 SS Disc = 47.2804 g; Diam of Disc = 5.08 cm

Time, hr	Bi-Sn Bath Composition				ΣC_i,*
	w/o Fe	w/o Cr	w/o Ni	w/o Mn	w/o 304 SS
0	<0.005	<0.005	<0.005	<0.0005	~0
0.66	0.034	0.012	0.008	0.0005	0.0545
1.0	0.051	0.019	0.013	0.0015	0.0845
2.0	0.082	0.026	0.015	0.002	0.125
3.0	0.092	0.023	0.015	0.003	0.133
4.0	0.170	0.057	0.033	0.004	0.264
5.0	0.170	0.058	0.034	0.003	0.265
6.0	0.160	0.050	0.035	0.004	0.249
22.0	0.320	0.120	0.073	0.010	0.523
26.0	0.300	0.120	0.080	0.010	0.510
30.0	0.290	0.130	0.086	0.010	0.516
75.0	0.240	0.160	0.110	0.015	0.525
94.0	0.260	0.160	0.110	0.014	0.544
100.0	0.230	0.170	0.120	0.015	0.535

*ΣC_i = sum of the concentrations of the four components of Type 304 stainless steel in the bismuth-tin bath.

Run No. 3

T = 650°C, 100 rpm | Weight of Bi-Sn Bath = 4498 g | Weight of 304 SS Disc = 47.8185 g | Diam of Disc = 5.08 cm

Time, hr	Bi-Sn Bath Composition				ΣC_i,*
	w/o Fe	w/o Cr	w/o Ni	w/o Mn	w/o 304 SS
0.5	<0.003	<0.0005	<0.0005	<0.0005	~0
1.0	<0.003	<0.0005	<0.0005	<0.0005	0
1.5	<0.003	<0.0005	<0.0005	<0.0005	0
2.0	<0.003	<0.0005	<0.0005	<0.0005	0
2.5	0.0049	<0.0005	<0.0005	<0.0005	0.0049
3.5	0.0060	<0.0005	<0.0005	<0.0005	0.0060
4.0	0.0085	0.0008	0.0007	<0.0005	0.0100
5.0	0.0087	0.0015	0.0010	<0.0005	0.0112
8.0	0.0142	0.0026	0.0016	<0.0005	0.0184
9.0	0.0168	0.0039	0.0023	<0.0005	0.0230
10.0	0.020	0.0060	0.0028	0.0006	0.0294
23.5	0.046	0.0140	0.0070	0.0010	0.0680
28.0	0.052	0.0137	0.0087	0.0013	0.0757
32.0	0.058	0.0149	0.0090	0.0013	0.0832
47.5	0.058	0.0168	0.0110	0.0013	0.0871
50.0	0.074	0.0190	0.0115	0.0011	0.1155

Run No. 4

T = 450°C, 100 rpm | Weight of Bi-Sn Bath = 4502 g | Weight of 304 SS Disc = 47.3877 g | Diam of Disc = 5.08 cm

Time, hr	Bi-Sn Bath Composition				ΣC_i,*
	w/o Fe	w/o Cr	w/o Ni	w/o Mn	w/o 304 SS
0.5	<0.0005	<0.0005	<0.0005	<0.0005	~0
1.0	<0.0005	<0.0005	<0.0005	<0.0005	~0
2.0	<0.0005	<0.0005	<0.0005	<0.0005	~0
3.0	<0.0005	<0.0005	<0.0005	<0.0005	~0
5.0	<0.0005	<0.0005	<0.0005	<0.0005	~0
6.0	<0.0005	<0.0005	<0.0005	<0.0005	~0
7.0	<0.0005	<0.0005	<0.0005	<0.0005	~0
8.0	<0.0005	<0.0005	<0.0005	<0.0005	~0
9.0	0.0039	<0.0005	<0.0005	<0.0005	0.0039
24.5	0.0068	0.0011	0.0008	<0.0005	0.0087
29.0	0.0076	0.0013	0.0009	<0.0005	0.0098
33.0	0.0106	0.0013	0.0010	<0.0005	0.0129
50.0	0.0093	0.0015	0.0012	<0.0005	0.0120

*ΣC_i = sum of the concentrations of the four components of Type 304 stainless steel in the bismuth-tin bath.

Run No. 5

T = 650°C, 10.0 rpm; Weight of Bi-Sn Bath = 4502 g; Weight of 304 SS Disc = 47.3877 g; Diam of Disc = 5.08 cm

Time, hr	Bi-Sn Bath Composition				ΣC_i,*
	w/o Fe	w/o Cr	w/o Ni	w/o Mn	w/o 304 SS
0.5	<0.003	<0.0005	<0.0005	<0.0005	~0
1.0	<0.003	<0.0005	<0.0005	<0.0005	~0
1.5	<0.003	<0.0005	<0.0005	<0.0005	~0
2.0	<0.003	<0.0005	<0.0005	<0.0005	~0
3.0	<0.003	<0.0005	<0.0005	<0.0005	~0
4.0	<0.003	<0.0005	<0.0005	<0.0005	~0
5.0	<0.003	<0.0005	<0.0005	<0.0005	~0
6.0	0.0053	0.0018	0.0010	<0.0005	0.0081
7.0	0.0042	0.0011	0.0010	<0.0005	0.0063
8.0	0.0042	0.0015	0.0008	<0.0005	0.0065
9.0	0.0058	0.0016	0.0015	0.0006	0.0095
24.0	0.0340	0.0102	0.0057	0.0011	0.0510
28.5	0.0324	0.0100	0.0050	0.0012	0.0486
32.5	0.0358	0.0100	0.0060	0.0010	0.0528
48.0	0.0560	0.0136	0.0082	0.0014	0.0692
72.0	0.0600	0.0184	0.0098	0.0017	0.0899
80.0	0.0680	0.0200	0.0104	0.0017	0.0901

Run No. 6

T = 860°C, 10.0 rpm; Weight of Bi-Sn Bath = 4476 g; Weight of 304 SS Disc = 47.4068 g; Diam of Disc = 5.08 cm

Time, hr	Bi-Sn Bath Composition				ΣC_i,*
	w/o Fe	w/o Cr	w/o Ni	w/o Mn	w/o 304 SS
0.5	0.0137	0.0053	0.0029	<0.0005	0.0190
1.0	0.0290	0.0110	0.0057	0.0011	0.0468
2.0	0.0560	0.0195	0.0123	0.0017	0.0895
3.0	0.0900	0.0248	0.0164	0.0024	0.1336
4.0	0.1420	0.0346	0.0228	0.0031	0.2025
5.0	0.1360	0.0392	0.0272	0.0046	0.2070
6.0	0.1640	0.0520	0.0304	0.0046	0.2510
7.0	0.1640	0.0508	0.0324	0.0052	0.2524
8.0	0.1920	0.0600	0.0368	0.0055	0.2943
9.0	0.196	0.0692	0.0376	0.0048	0.3076
10.0	0.212	0.0692	0.0368	0.0049	0.3229

*ΣC_i = sum of the concentrations of the four components of Type 304 stainless steel in the bismuth-tin bath.

Run No. 6 (Contd.)

Time, hr	Bi-Sn Bath Composition				ΣC_i,*
	w/o Fe	w/o Cr	w/o Ni	w/o Mn	w/o 304 SS
24.0	0.305	0.110	0.0615	0.0073	0.4838
28.0	0.233	0.082	0.062	0.0082	0.3852
48.0	0.233	0.085	0.074	0.0094	0.4014
52.0	0.215	0.105	0.084	0.0108	0.4148
56.0	0.227	0.096	0.073	0.0104	0.4064
72.0	0.195	0.106	0.091	0.0130	0.4050
100.0	0.258	0.139	0.101	0.0136	0.5116

Run No. 7

T = 750°C Weight of Bi-Sn Weight of 304 SS Disc Diam of Disc
10.0 rpm Bath = 4483 g = 45.8062 g = 5.08 cm

Time, hr	Bi-Sn Bath Composition				ΣC_i,*
	w/o Fe	w/o Cr	w/o Ni	w/o Mn	w/o 304 SS
0.5	<0.003	<0.0005	<0.0005	<0.0005	~0
1.0	<0.003	<0.0005	<0.0005	<0.0005	~0
2.0	<0.003	<0.0005	<0.0005	<0.0005	~0
3.0	0.0031	0.0014	0.0013	<0.0005	0.0058
4.5	0.0077	0.0031	0.0020	<0.0005	0.0128
7.0	0.0485	0.0134	0.0095	0.0012	0.0726
8.0	0.0550	0.0160	0.0114	0.0018	0.0842
10.0	0.0990	0.0335	0.0195	0.0027	0.1547
24.25	0.1340	0.0555	0.0375	0.0043	0.2313
32.5	0.1075	0.0450	0.0345	0.0049	0.1919
48.0	0.1320	0.0570	0.0465	0.0076	0.2431
52.5	0.1500	0.0670	0.0585	0.0083	0.2838
100.0	0.1530	0.0910	0.0780	0.0128	0.3348
150.0	0.1460	0.0830	0.0905	0.0135	0.3330

*ΣC_i = sum of the concentrations of the four components of Type 304 stainless steel in the bismuth-tin bath

Run No. 8

T = 860°C, 2.0 rpm; Weight of Bi-Sn Bath = 4463 g; Weight of 304 SS Disc = 46.7888 g; Diam of Disc = 5.08 cm

Time, hr	Bi-Sn Bath Composition w/o Fe	w/o Cr	w/o Ni	w/o Mn	ΣC_i,* w/o 304 SS
0.5	0.0083	0.0035	0.0026	<0.0005	0.0144
1.0	0.0132	0.0041	0.0034	0.0005	0.0212
2.0	0.0301	0.0126	0.0075	0.0008	0.0510
3.5	0.0450	0.0164	0.0088	0.0013	0.0715
5.0	0.051	0.0142	0.0092	0.0012	0.0756
6.0	0.053	0.0161	0.0100	0.0014	0.0805
7.0	0.069	0.0286	0.0252	0.0034	0.1262
8.0	0.067	0.0286	0.0176	0.0024	0.1156
9.0	0.068	0.0338	0.0190	0.0027	0.1235
10.0	0.106	0.0480	0.0224	0.0032	0.1796
24.0	0.226	0.086	0.0550	0.0076	0.3746
35.0	0.264	0.095	0.0610	0.0085	0.4485
48.0	0.240	0.110	0.0805	0.0129	0.4434
72.0	0.350	0.117	0.0840	0.0096	0.5606
127.0	0.274	0.114	0.112	0.0143	0.5143
150.0	0.276	0.126	0.102	0.0136	0.5176

Run Nos. 9 and 11 Combined Data

T = 860°C, 30.0 rpm; Weight of Bi-Sn Bath = 4500 and 4502 g; Weight of 304 SS Discs = 46.8741 g (9) and 45.6558 g (11); Diam of Discs = 5.08 cm

Time, hr	Bi-Sn Bath Composition w/o Fe	w/o Cr	w/o Ni	w/o Mn	ΣC_i,* w/o 304 SS
0.5	<0.005	<0.001	<0.001	<0.0005	~0
1.0	<0.005	<0.001	<0.001	<0.0005	~0
2.0	<0.005	<0.001	<0.001	<0.0005	~0
3.0	0.0190	0.0057	0.0031	0.0005	0.0283
4.5	0.0555	0.0165	0.0100	0.0014	0.0834
5.0	0.0560	0.0184	0.0088	0.0017	0.0849
6.0	0.1120	0.0324	0.0189	0.0023	0.1656
6.0	0.1160	0.0356	0.0276	0.0042	0.1834
7.0	0.1720	0.0490	0.0258	0.0037	0.2505
8.0	0.2040	0.0452	0.0302	0.0045	0.2859
10.0	0.2850	0.0765	0.0375	0.0060	0.4050

*ΣC_i = sum of the concentrations of the four components from Type 304 stainless steel in the bismuth-tin bath.

Run Nos. 9 and 11 Combined Data (Contd.)

Time, hr	Bi-Sn Bath Composition w/o Fe	w/o Cr	w/o Ni	w/o Mn	ΣC_i,* w/o 304 SS
10.0	0.2040	0.0740	0.0500	0.0063	0.3343
24.0	0.2765	0.0945	0.0585	0.0084	0.4379
25.0	0.2580	0.1100	0.0705	0.0082	0.4467
150.0	0.2650	0.1330	0.1110	0.0169	0.5259

Run No. 10

T = 860°C, 150 rpm; Weight of Bi-Sn Bath = 4501 g; Weight of 304 SS Disc = 45.4446 g; Diam of Disc = 5.08 cm

Time, hr	Bi-Sn Bath Composition w/o Fe	w/o Cr	w/o Ni	w/o Mn	ΣC_i,* w/o 304 SS
0.5	0.0275	0.0080	0.0047	0.0004	0.0406
1.0	0.0640	0.0160	0.0109	0.0010	0.0919
2.0	0.1100	0.0282	0.0203	0.0019	0.1604
4.0	0.1590	0.0635	0.0360	0.0045	0.2630
5.0	0.2140	0.0635	0.0394	0.0046	0.3215
6.0	0.2290	0.0635	0.0446	0.0061	0.3432
8.0	0.2450	0.0795	0.0550	0.0069	0.3864
10.0	0.2500	0.0850	0.0640	0.0078	0.4068
24.0	0.3130	0.1260	0.0900	0.0119	0.5409
30.0	0.290	0.1160	0.0920	0.0125	0.5105
56.0	0.290	0.1250	0.0910	0.0119	0.5079
72.0	0.315	0.1350	0.1200	0.0150	0.5850
100.0	0.320	0.1380	0.1180	0.0170	0.5930

Run No. 12

T = 860°C, 20.0 rpm; Weight of Bi-Sn Bath = 4503 g; Weight of 304 SS Disc = 47.1795 g; Diam of Disc = 5.08 cm

Samples were not submitted for chemical analysis because of problems encountered with disc rotation during the run.

*ΣC_i = sum of the concentrations of the four components of Type 304 stainless steel in the bismuth-tin bath.

Run No. 13

T = 860°C, 50.0 rpm; Weight of Bi-Sn Bath = 4500 g; Weight of 304 SS Disc = 46.7014 g; Diam of Disc = 5.08 cm

Time, hr	Bi-Sn Bath Composition				ΣC_i,* w/o 304 SS
	w/o Fe	w/o Cr	w/o Ni	w/o Mn	
0.5	<0.001	<0.001	<0.001	<0.0005	~0
1.0	<0.001	<0.001	<0.001	<0.0005	~0
2.5	<0.001	0.0042	0.0026	<0.0005	0.0068
3.0	0.0475	0.0111	0.0071	0.0009	0.0066
4.0	0.0770	0.0191	0.0109	0.0013	0.1083
4.5	0.0740	0.0202	0.0143	0.0019	0.1104
5.5	0.0970	0.0244	0.0161	0.0022	0.1397
6.0	0.1270	0.0382	0.0295	0.0023	0.1970
8.0	0.1480	0.0416	0.0344	0.0041	0.2281
10.0	0.1775	0.0510	0.0393	0.0048	0.2726
24.0	0.2708	0.0785	0.0733	0.0074	0.4300
30.0	0.2558	0.0798	0.0775	0.0089	0.4170
32.0	0.2763	0.0920	0.0713	0.0086	0.4482
50.0	0.2553	0.0905	0.0880	0.0109	0.4447

Run No. 14

T = 860°C, 30.0 rpm; Weight of Bi-Sn Bath = 3349 g; Weight of 304 SS Disc = 48.3714 g; Diam of Disc = 5.08 cm

Samples were not submitted for chemical analysis because of problems encountered with disc rotation during the run.

Run No. 15**

T = 860°C, 30.0 rpm; Weight of Bi-Sn Bath = 4503 g; Weight of 304 SS Disc = 47.1795 g; Diam of Disc = 5.08 cm

Time, hr	Bi-Sn Bath Composition				ΣC_i,* w/o 304 SS
	w/o Fe	w/o Cr	w/o Ni	w/o Mn	
1.0	0.2975	0.0850	0.0800	0.0059	0.4684
2.0	0.2390	0.0635	0.0740	0.0045	0.3710
4.5	0.3090	0.0900	0.0810	0.0066	0.4866

*ΣC_i = sum of the concentrations of the four components from Type 304 stainless steel in the bismuth-tin bath.

**The disc was lowered into the bath at a temperature of 300°C. Ten hours later, the system reached 860°C and was at temperature for 3.5 hr prior to setting the rotational speed to 30 rpm.

Run No. 15** (Contd.)

Time, hr	Bi-Sn Bath Composition w/o Fe	w/o Cr	w/o Ni	w/o Mn	ΣC_i,* w/o 304 SS
6.75	0.2675	0.0815	0.0825	0.0042	0.4357
9.0	0.2975	0.0885	0.0810	0.0059	0.4729
30.0	0.4050	0.1350	0.1225	0.0116	0.6741
79.0	0.3730	0.1500	0.1330	0.0162	0.6722

Run No. 16

T = 1100°C, 10.0 rpm; Weight of Bi-Sn Bath = 2700 g; Weight of 304 SS Disc = 48.0533 g; Diam of Disc = 5.08 cm

Time, hr	Bi-Sn Bath Composition w/o Fe	w/o Cr	w/o Ni	w/o Mn	ΣC_i,* w/o 304 SS
0.0	0.060	0.0192	0.0315	0.0011	0.1118
0.25	0.2285	0.0820	0.0700	0.0049	0.3854
0.50	0.2925	0.0955	0.0805	0.0073	0.4758
1.0	0.4165	0.1425	0.1105	0.0116	0.6711
2.0	0.6640	0.1960	0.1420	0.0140	1.0160
3.0	0.8500	0.2360	0.1730	0.0178	1.2768
3.5	0.8700	0.2620	0.1860	0.0213	1.3393
4.0	1.0400	0.2740	0.1860	0.0214	1.5214
6.0	0.9150	0.2960	0.1800	0.0257	1.4167

Run No. 17

T = 1050°C, 10.0 rpm; Weight of Bi-Sn Bath = 2700 g; Weight of 304 SS Disc = 47.7780 g; Diam of Disc = 5.08 cm

Time, hr	Bi-Sn Bath Composition w/o Fe	w/o Cr	w/o Ni	w/o Mn	ΣC_i,* w/o 304 SS
0.0	<0.0005	<0.0005	<0.0005	<0.0005	~0
0.25	0.0670	0.0210	0.0098	0.0014	0.0992
0.75	0.2185	0.0675	0.0390	0.0063	0.3313

*ΣC_i = sum of the concentrations of the four components from Type 304 stainless steel in the bismuth-tin bath.

**The disc was lowered into the bath at a temperature of 300°C. Ten hours later, the system reached 860°C and was at temperature for 3.5 hr prior to setting the rotational speed to 30 rpm.

Run No. 17 (Contd.)

Time, hr	Bi-Sn Bath Composition				ΣC_i,*
	w/o Fe	w/o Cr	w/o Ni	w/o Mn	w/o 304 SS
1.00	0.3700	0.1035	0.0620	0.0146	0.5501
1.50	0.555	0.1585	0.0720	0.0116	0.7971
2.0	0.625	0.1850	0.0940	0.0120	0.9160
2.5	0.640	0.2010	0.0845	0.0125	0.9380
3.0	0.688	0.2180	0.1100	0.0152	1.0312
3.5	0.710	0.2320	0.1080	0.0162	1.0662
4.0	0.810	0.2670	0.1285	0.0160	1.2215
4.5	0.720	0.2560	0.1080	0.0144	1.0884
5.0	0.780	0.2740	0.1355	0.0081	1.1976
6.0	0.790	0.2590	0.1260	0.0100	1.1850
7.0	0.733	0.2540	0.1350	0.0105	1.1325
24.0	0.816	0.2740	0.1500	0.0100	1.2500
31.0	0.890	0.3270	0.1690	0.0111	1.3971
51.5	0.850	0.2970	0.1650	0.0100	1.3220

*ΣC_i = sum of the concentrations of the four components from Type 304 stainless steel in the bismuth-tin bath.

APPENDIX C

Equilibrium-solubility Data for 304 SS in the Bi-42w/oSn Eutectic Alloy

Temp, °C	Bath Composition				Equilibration Time, hr
	w/o Fe	w/o Cr	w/o Ni	w/o Mn	
450	< 0.005	0.0058	0.0060	< 0.0005	~426
	< 0.005	0.0044	0.0058	< 0.0005	
	< 0.005	0.0051	0.0055	< 0.0005	
650	0.0587	0.0572	0.1425	0.0147	~500
	0.0475	0.0610	0.1040	0.0129	
	0.0727	0.0595	0.1084	0.0125	
860	0.2735	0.2050	0.7740	0.0772	~500
	0.2290	0.2180	0.7520	0.0892	
	0.2700	0.2650	0.8890	0.0932	
985	0.6080	0.3870	*	*	~190
	0.4700	0.4090			
	0.5125	0.3880			
1050	0.8110**				~55
1100	0.9350**				6

*Saturation with respect to nickel and manganese may not have been attained.

**Values from the dissolution curves for iron in Runs 16 and 17.

ACKNOWLEDGMENT

The author wishes to thank E. A. Huff and S. J. Kulpa of the Chemistry Division for performing the spectrochemical analysis on the numerous samples submitted. Thanks are also extended to D. L. Rink for help with the experimental work and to D. A. Woodward and J. B. Herman of the Applied Mathematics Division for providing the computer integration results for Equation (26).

REFERENCES

1. L. L. Bircumshaw and A. C. Riddiford, Quarterly Reviews 6, 157-185 (1952).
2. A. G. Ward and J. W. Taylor, J. Inst. Metals 85, 145-152 (1956).
3. A. G. Ward and J. W. Taylor, J. Inst. Metals 86, 36-42 (1957).
4. D. A. Stevenson and J. Wulff, Trans. Met. Soc. AIME 221, 279-285 (1961).
5. J. K. Jackson and R. E. Grace, International Symposium on the Physical Chemistry of Process Metallurgy, Met. Soc. AIME 7, I, 633-644 (1961).
6. E. A. Moelwyn-Hughes, The Kinetics of Reactions in Solutions, 2nd ed., Oxford Univ. Press, New York, 1947, p. 374.
7. V. G. Levich, Discussions of the Faraday Soc. 1, 37-42 (1947).
8. V. G. Levich, Physicochemical Hydrodynamics, 2nd ed., Prentice Hall, Inc., Englewood Cliffs, N. J., 1962.
9. W. G. Cochran, Proc. of the Cambridge Phil. Soc. 30, 365-375 (1934).
10. Th. von Karman, National Advisory Comm. Aeronaut., TM-1092, (1946).
11. E. M. Sparrow and J. L. Gregg, Journal of Heat Transfer 81C, 249-251 (1959).
12. D. P. Gregory and A. C. Riddiford, J. Chem. Soc., London, 731, 3756-3764 (1956).
13. F. Sauerwald and K. Töpler, Zeitschrift fur anorganische und allgemeine Chemie 157, 117-137 (1926).
14. R. A. Swalin, Acta Met. 7, 736-740 (1959).
15. H. A. Walls and W. R. Upthegrove, Acta Met. 12, 461-471 (1964).
16. T. F. Kassner, R. J. Russel and R. E. Grace, Trans. Am. Soc. Metals 55, 858-865 (1962).
17. J. D. Harrison and C. Wagner, Acta Met. 7, 722-735 (1959).